Time Resolved Study of Femtosecond Microfabrication In Silica Glass

Hiroaki Misawa[a], Saulius Juodkazis,[a] Andrius Marcinkevičius,[b] Mitsuru Watanabe,[a]
Vygantas Mizeikis,[b] and Shigeki Matsuo,[a]

[a]Department of Ecosystem Engineering, The University of Tokushima,
2-1 Minamijyosanjima, Tokushima 770-8506, Japan
[b]Laboratory of Nano-Photonic Materials, The University of Tokushima,
2-1 Minamijyosanjima, Tokushima 770-8506, Japan

ABSTRACT

We report investigation of light-induced damage threshold (LIDT) in purified silica (transmission band down to 160 nm) by 350 fs laser pulses at the wavelength of 795 nm and 498 nm. Focusing a single pulse by a high numeric aperture $NA = 1.35$ microscope objective lens results in one of the lowest single-shot bulk LIDT values reported so far, 5 J/cm^2, while the surface ablation threshold is 2.5 J/cm^2 with both values being well below the critical self-focusing power in silica. Furthermore, we report the peculiarities of damage by two-pulse irradiation (duration of each pulse is 440 fs), where both pulses have energies at the level of $0.5 \times LIDT$. Comparison between the experimental data and numeric simulation, which takes into account optical free-carrier generation and relaxation, demonstrates that these processes can explain the measured self-focusing, super-continuum generation, and light-induced damage threshold values. We argue that use of high numeric aperture objective, despite substantial temporal pulse stretching, results in tight focusing which is capable of overcoming the beam self-focusing, and the resulting fabrication quality is comparable to that obtained using shorter pulses.

Keywords: laser microfabrication, light-induced damage threshold, silica

1. INTRODUCTION

Three-dimensional microstructuring in the bulk of transparent materials by high intensity fs laser pulses typically uses optical microscope, which produces strongly focused laser beams. Under these circumstances light-material interaction differs strongly from that encountered in the case of surface laser ablation. One particular issue, important for making the femtosecond fabrication more practical and cost-effective is the reduction of the photo-modification intensity threshold. To clarify this issue, and fully exploit the possibilities of 3D fabrication, the dynamics of dielectric breakdown occuring in the bulk within a tiny volume with sub-μm radius over sub-ps timescale must be revealed. Numerous earlier investigations of the interaction of intense laser radiation with transparent solids have focused on the dependence of the surface damage threshold on the pulsewidth in various materials,[1–3] while the role of multiphoton and avalanche ionization have been studied in.[4–6]

Dielectric breakdown through the optical absorption of laser radiation is due to partial or complete ionization of the material, usually treated as a consequence of i) multiphoton ionization coupled with tunneling, causing the excitation of electrons into the conduction band, ii) electron-electron collisional ionization due to the Joule heating, iii) transfer of the plasma energy to the lattice. In the first two processes, energy from the laser radiation is transferred to the free carrier plasma, while the third process releases plasma energy to the lattice, thus inducing permanent damage. Vaidyanathan *et al.*[7] emphasize that in many cases when ionization potential $\Delta \simeq 4\hbar\omega$, strength of the damage field predicted by the Keldysh multiphoton absorption formula is smaller than that resulting from the avalanche model, and is in close agreement with the experimental value. Moreover, these observations are inconsistent with Blombergen's hypothesis, according to which the multiphoton absorption would be the dominant mechanism for the laser-induced damage for photon energies exceeding half of the bandgap energy.[8] Stuart *et al.*[4] have shown

Author information:
S.J. and V.M: On leave from: Institute of Material Research and Applied Science, Vilnius University, Sauletekio 10, Vilnius 2054, Lithuania, E-mail address of S.J.: saulius@svbl.tokushima-u.ac.jp
H.M.: Corresponding author. E-mail address: misawa@eco.tokushima-u.ac.jp

Laser Applications in Microelectronic and Optoelectronic Manufacturing VI,
Malcolm C. Gower, Henry Helvajian, Koji Sugioka, Jan J. Dubowski, Editors,
Proceedings of SPIE Vol. 4274 (2001) © 2001 SPIE · 0277-786X/01/$15.00

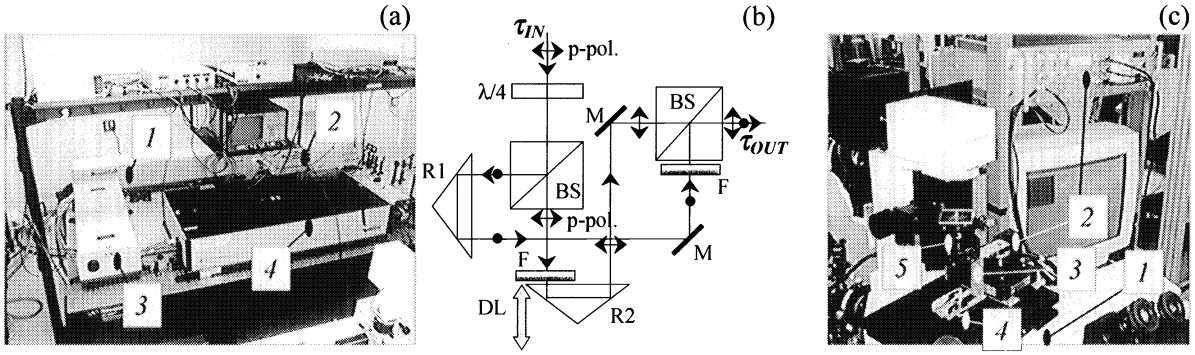

Figure 1. Laser setup (a), where *1* is the Ar-ion laser, *2* is the Ti:sapphire fs-oscilator, *3* YLF:Nd laser, which is pumping the reginerative amplifier *4*. (b) The two separated delayed pulses for two-pulse LIDT measurements were obtained using this setup: R1 and R2 are the broadband hollow retro-reflectors. R2 is mounted on a high precision delay line DL with 2 fs resolution, M are the mirrors, F are the metallic variable neutral density filters, and $\lambda/4$ is the quarter-wave plate. (c) Fabrication was done at the focal point of the microscope *1*. *2* is a high precission PZT stage and its driver, *3* - sample holder, *4* - objective lens, and *5* - condensor.

that if the multiphoton ionization occurs during the pulse propagation and the excited free electrons further seed the electron avalanche, the rate-equation approach can be used to obtain the electron density, which determines the ablation threshold. Recent results confirm that this model of optical breakdown is valid in general, but the nature and relative role of the electron avalanche and photoionization still remain controversial. Also, it should be noticed, that tunneling ionization can contribute to the free-carrier excitation, especially in the case of pulses shorter than ~100 fs. However, only few experimental and theoretical investigations were performed on the light-induced damage mechanism in the bulk of silica.[1,9,10] One of the possible reasons for this situation is in the fact that great care must be taken to avoid the self-focusing, which can significantly alter the experimentally determined values of LIDT for subpicosecond pulses. Use of high numerical aperture microscope lens for the pulse focusing gives a possiblity to overcome this problem.[10,11] Such focusing conditions allow to reach a single-shot LIDT at much lower power levels then in the case of self-focusing. The critical self-focusing power for the silica glass is about 3.92 MW, whereas the laser peak power in our experiments was just 0.74 MW even at 10×LIDT. Therefore, we do not need to take the self-focusing into account in the numeric simulations.

It is important to note, that fast (femtosecond) and slow (longer than picoseconds) relaxation processes can be exploited to lower the photo-modification threshold in the experiments using two beam irradiation. In silica, both sub-ps (0.2 ps[12,13]) and extremely long ns-ms (comparable to the lifetime of self-trapped excitons[14]) relaxations are reported. The second pulse can effectively launch an avalanche, which will eventually reach the light-induced damage threshold (LIDT or dielectric breakdown) of the material, provided that the free carriers (electrons and holes) seeded by the first pulse, are present. The role of the holes in multiphoton absorption and in the avalanche formation has not yet been addressed properly. It was demonstrated recently, that hole decay in O 2s level can generate two pairs of excitons in silica.[15]

In this work we report the reduction of LIDT in silica when two pulses are used for the damaging, and demonstrate the possibility to reduce LIDT by increasing the lattice temperature.

2. EXPERIMENTAL SETUP FOR TWO CONSECUTIVE PULSE IRRADIATION

The experimental setup for LIDT measurements consists of a Ti:sapphire laser with regenerative amplifier (Spectra Physics) and a microscope (Olympus IX70 or Nikon Otiphot-2). Typical pulse energy of the laser system is 0.5 mJ, duration 100-120 fs (FWHM) at the fundamental wavelength of 795 nm. The pulse is then split into two mutually delayed pulses using the setup shown in Fig. 1. The mechanical precision of the delay stage (500 nm) allows to achieve 2 fs temporal resolution, while broad delay range is ensured by the possibility to use coarse translation of the delay stage. The two pulses are introduced co-axially into the microscope, where they are focused by 100× magnification and $NA = 0.5 - 1.35$ numerical aperture objective lens. We carefully estimated the temporal pulse

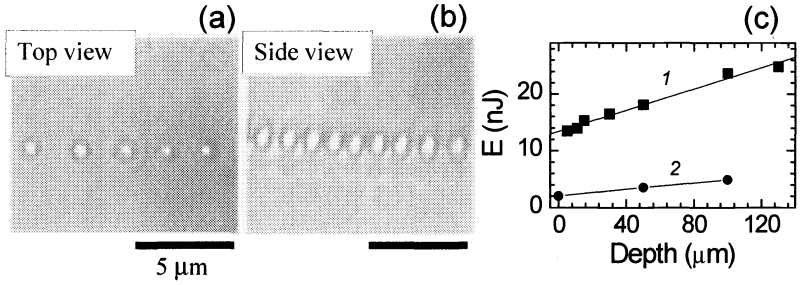

Figure 2. Top (a) and side (b) views of a single-pulse irradiated spot at fluence of $1.3 \times LIDT(1)$ at 795 nm wavelength in silica. (c) LIDT pulse energy dependence on the depth of focal point inside ED-C silica. Irradiation wavelength was 795 nm (*1*) and 398 nm (*2*). Focusing was made by objective lens of $NA = 1.35$.

spreading induced by the optical elements used in the setup. In our experiments we used polarizing beam splitters (BS in Fig. 1) made from highly dispersive BK-7 optical glass. The eventual pulse duration at the entrance to the microscope is about 430 fs, while the microscope alone broadens the laser pulse to about 350 fs. Thus, the actual pulse duration at the irradiation site is about 440 fs in the two-pulse LIDT experiments at 795 nm wavelength.

Temporal coincidence of the pulses was checked using co-linear second harmonic generation in a 1 mm thick BBO crystal (I^{st} phase-matching type). The optical axis of the crystal was oriented at 45° with respect to the plane of the incident beam polarization. This allowed to fix the temporal overlap of the two pulses within 0.4 ps ccuracy. Direct observation of the spatial (lateral and axial) coincidence of the two pulses with the microscope was done by luminescence visualization of the beam, focused in the rhodamine dye solution. The spatial overlap was fixed with precision better than 0.3 μm, and was also checked by monitoring the damage inflicted by each pulse separately at the power level of $LIDT$. The temporal overlap in the case of 398 nm wavelength was checked by observing the signal generated by two pulse interference pattern on a photodiode. The two cross-polarized pulses were passed through the polarizer oriented at 45^0 with respect to the polarizations of both pulses and were incident on the photodiode. The temporal overlap was set with the accuracy of 0.4 ps.

Temperature dependence of LIDT was measured using a *Linkam-1500* annealing chamber mounted on the *Nikon Optiphot-2* microscope. The setup allows to heat the sample up to the temperature of 1500°C, while irradiating and monitoring it with 40× magnification objective lens of $NA = 0.55$.

In our experiments we used low contamination silica, ED-C brand, from Nippon Silica Glass (OH concentration less than 1 ppm, Cl $\leq$ 830 ppm) with transmission band down to 160 nm (transmission at 50% shown). Synthetic ED-C silica was made by a vapor-phase axial deposition (VAD), a kind of soot remelting technology. Effective bandgap of ED-C silica was evaluated from the dependence $\alpha \propto \sqrt{h\nu}$, which is valid for direct transitions, and yields Δ=7.4 eV. Such estimate assumes direct optical transitions between the density of states tails in amorphous materials.

3. RESULTS AND DISCUSSION

3.1. Definition of Light Induced Damage Threshold for N pulses ($LIDT(N)$)

Large number of experimental and theoretical studies have been devoted to determine LIDT in various materials. The recent experimental data in silica are summarized in Table 1. The discrepancy seen in the experimental results may arise from the different techniques of LIDT determination. So far the most popular laser-induced damage definition techniques are: i) light scattering at the irradiation point, ii) plasma emission (white continuum generation), iii) observation of any visible permanent sample modifications with Nomarski-type microscope. Quoix *et al.*[18] have demonstrated the possibility to study the breakdown study by using frequency domain interferometry (FDI).

In our work, determination of single pulse LIDT was done by direct *in situ* optical observation in the microscope with about 398 nm spatial resolution using $NA = 1.35$ objective lens (i.e. the lateral resolution attainable with condenser illumination of the fabricated spot). Typical images are presented in Fig.2(a,b). Hereinafter $LIDT(1)$ refers to the single pulse LIDT, while $LIDT(2)$ refers to the double pulse LIDT. The LIDT was determined as the

Table 1. Dielectric breakdown thresholds in silica.

Pulse duration, fs	Wavelength, nm	F_{th}, J/cm^2	Detection method	Remarks	Source
20	780	2	Scattering	single-shot, surface	Ref. 2
25	800	1.5	Continuum generation	single-shot, surface	Ref. 12
100	800	3.9	Optical microscope	single-shot, bulk	Ref. 16
100	800	2.89	Scattering	multi-shot, bulk	
100	800	3.8	Nomarski microscope	single-shot, surface	Ref. 17
100	800	0.9	Nomarski microscope	multi-shot, surface	
150	825	1.8	Nomarski microscope	multi-shot, surface	Ref. 4
200	800	2	Nomarski microscope	Single-shot, surface	Ref. 3
200	800	11	Continuum generation	Single-shot, bulk	Ref. 1
760	800	1.7	FDI	Single-shot, surface	Ref. 18
350	795	5	Optical microscope	Single-shot, bulk*	Present study
350	795	2.5	Optical microscope	Single-shot, surface	
350	795	4.5	Optical microscope	Multi-shot, bulk*	
440	795	6.9	Optical microscope	Single-shot, bulk*	

* Measured at 100 μm depth.

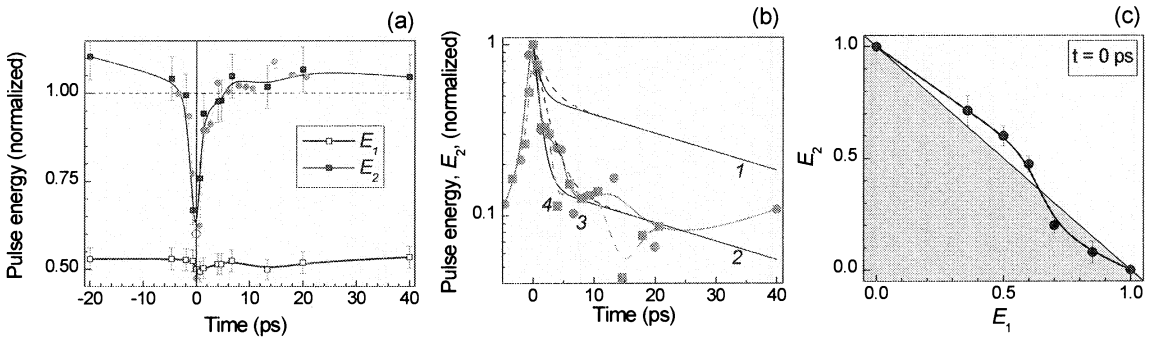

Figure 3. Optical damaging of ED-C silica with two fs-pulses separated in time. (a) The dependence of second pulse energy, E_2, on the time delay between the two pulses at different ratio E_2/E_1 ($E_1 = 0.5 \times LIDT(1)$ black and $E_1 = 0.4 \times LIDT(1)$ - grey markers). The energy of the first sub-threshold pulse, E_1, was constant. The pulse energies are normalized to the single-shot $LIDT(1) = 32.6$ nJ of silica. (b) Simulated two-exponential decay were calculated by $y = 0.5(e^{-x/\tau_1} + e^{-x/\tau_2})$ (*1*) and $y = 0.85e^{-x/\tau_1} + 0.15e^{-x/\tau_2}$ (*2*). The time constants were 1 and 40 ps (solid-black line) and 2 and 40 ps (dashed-black line), respectively. Experimental LIDT recovery data presented as $(1 - E_2)$ (given by *3,4*; data are taken from (a)). (c) Verification of the dependence $E_1 + E_2 = LIDT(1) \equiv 1$. The grey region depicts the area where $LIDT(2) < LIDT(1)$ in silica. Experimental data are connected by lines, which are drawn as a visual aid only.

power level at which 75% of all laser shots leave observable change in the optical contrast in the sample. This definition enabled us to determine LIDT values more than 2 times lower, compared to those reported by Du *et al.*.[1] The single-shot bulk LIDT fluence was 5 J/cm^2 for the 350 fs pulses (see Table 1). The LIDT(1) value on the surface was measured to be 2.5 J/cm^2, half of the bulk value at 100 μm, and is among the lowest values measured in silica (Table 1). This infers that sensitivity of the technique is sufficient to determine inherent LIDT of silica.

3.2. Two consecutive pulse damaging of silica at 795 nm

First, we address the question whether LIDT for multi-shot excitation is smaller than for single-shot excitation. If the first laser pulse with sub-threshold energy $E_1 < LIDT(1)$ modifies material to a degree sufficient to decrease the LIDT value, then the second pulse can induce optical damage at $E_2 < LIDT(1) - E_1$. From the simulation of free-carrier generation (see Sect. 3.5 for details) the following scenario is expected. The first pulse at $0.5 \times LIDT$

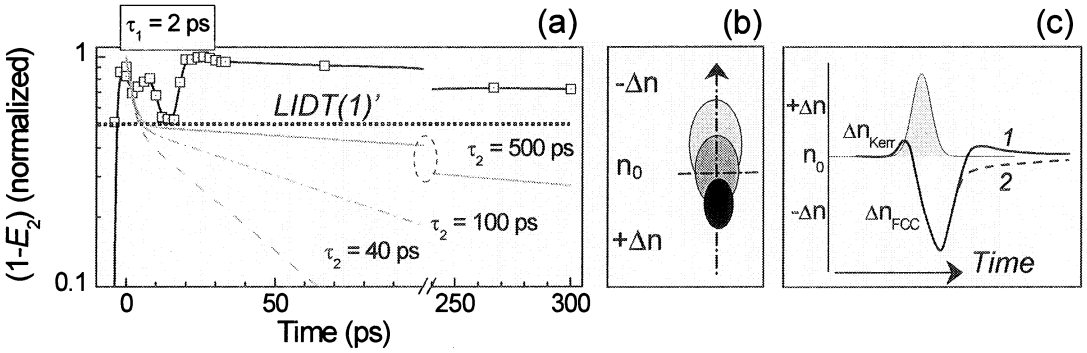

Figure 4. (a) Time dependency of $(1-E_2)$ (normalized to its maximum), when $E_1 \simeq LIDT(1)$ at 795 nm wavelength. No damage was recorded by the first pulse even at this fluence of $LIDT(1)$ due to the slight defocusing. The new level of $LIDT(1)'$ is given by dotted line. Simulated time decays (grey lines) are calculated by $y = 0.5(e^{-x/\tau_1} + e^{-x/\tau_2})$, where $\tau_1 = 2$ ps and $\tau_2 = 40$; 100; 500 ps, respectively (grey lines). (b) Schematic presentation of axial cross-section of the focal point along the optical axis (the light propagation is shown by the arrow). Any change of refractive index $\pm\Delta n$ causes change in the spot size and location. (c) Presentation of the expected time dependence of the change in refraction index. Temporal profile of Gaussian excitation pulse is given by gray-shaded area (c).

creates some density of free conduction electrons below the critical LIDT density. The electron density peaks after about 300 fs, and subsequently decays. The second delayed pulse interacts with the excited free carriers, and thus less energy is required in order to reach the critical density at zero delay between the two pulses. With increasing delay, density of electrons, left in the conduction band after the first pulse decreases due to the relaxation (such as free-carrier scattering, fast nonlinear diffusion, all types of free-carriers capture and recombination), and therefore higher pulse energy is required for reaching LIDT. For long delays the material recovers totaly after the first pulse and one-pulse LIDT(1) is required for achieving damage.

Results. These theoretical predictions were checked experimentally by optical damaging with two cross-polarized fs-pulses. Cross-polarized irradiation allows to avoid interference effects, which may decrease the accuracy of the LIDT determination. In the two-pulse experiments the energy of the first pulse E_1 was fixed at certain level below $LIDT(1)$, and below is expressed in the units of $LIDT(1)$, while the energy of the second delayed pulse E_2 was adjusted for each delay to the level required to reach the optical breakdown, i.e. $LIDT(2)$. For positive delays the fixed-energy pulse E_1 precedes the delayed one. The absolute value of LIDT(1) was found to be 6.9 J/cm^2 (Table 1).

In two-pulse experiments we have observed increase in LIDT for delays between 1 and 2 ps (Fig. 3(a,b)). The actual pulse duration inside the sample was 440 fs. Fig. 3(b) depicts the same data as in Fig. 3(a), but given as the normalized recovery time of silica LIDT. In fact, no decrease in LIDT(2) occurrs, i.e. $E_1 + E_2 = LIDT(1) \equiv 1$ as compared with that for a single pulse ($LIDT(1)$). LIDT recovery of silica can be well approximated by a two-exponential decay (Fig. 3(b)), with the fast time constant being $\tau_1 = 1 \sim 2$ ps. Fig. 3(c) shows the dependence of the delayed beam energy E_2 on the fixed beam energy E_1. All data points were measured at zero delay between the pulses.

The data in Fig. 3 were obtained when the pulse spatial overlap and their alignment along the optical axis of the microscope was fully optimized, i.e. at the smallest focal volume. Under these conditions, the lowest LIDT were observed. The prevailing source of uncertainty in the two-pulse optical damaging experiments is beam misalignment, which affects axial overlap of the pulses. Signatures of two pulses not coinciding spatially are the increase in the values of LIDT, and "erasure", or recovery of the observable transmision changes (made by the first pulse) after the irradiation by the second pulse. This phenomenon was reported recently[19] and is particularly important for negative delays, where increase of LIDT(2) was up to 200%. We have deliberately introduced misalignment between the two pulses to reach $LIDT(1)' = 51$ nJ $> LIDT(1)$. Then, the experiment was carried out with $E_1 = 0.7 \times LIDT(1)' = const$. The results are shown in Fig. 4. Instead of LIDT recovery, more complex temporal evolution was observed. One of the most feasible causes for this is the heating in the focal spot, which is more significant in this experiment as compared with the data presented in Fig. 3. The overall energy delivered to the

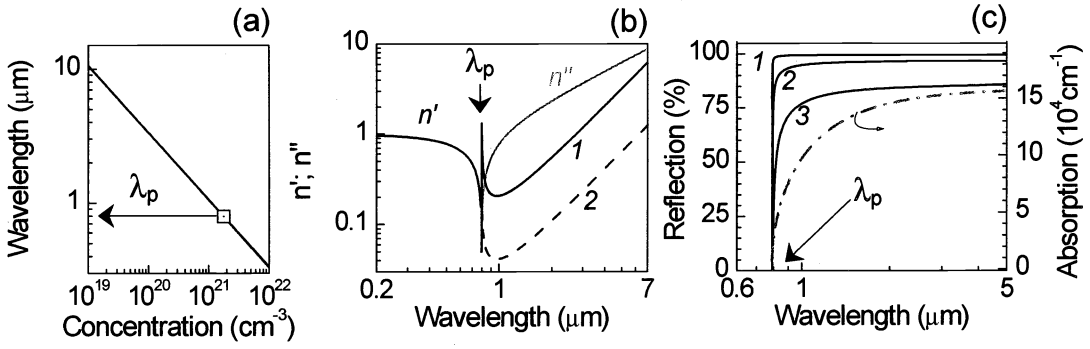

Figure 5. (a) Dependence of plasmon wavelength on the free carrier concentration. (b) Complex refraction index $\tilde{n}(\omega) = n'(\omega) + in''(\omega)$ vs. wavelength λ ($\omega = 2\pi\lambda/c$) according to eqns. 3 and 4. Spectra of free carriers plasma at concentration of 1.77×10^{21} cm^{-3} calculated for a fast electron-phonon interaction equal to the plasmon frequency $\nu = \omega_p/2\pi$ (*1*) and at $\nu = (\omega_p/2\pi)/5$ (*2*). (c) Reflection and absorption at free carrier concentration of 1.77×10^{21} cm^{-3} (corresponding plasmon wavelength $\lambda_p = 793$ nm). The reflection is calculated for different relaxation rates: $\nu = (\omega_p/2\pi)/100$ (*1*), $(\omega_p/2\pi)/10$ (*2*), and $(\omega_p/2\pi)/5$ (*3*).

focal region is several times larger than that in the case of perfectly aligned setup. The influence of temperature on LIDT is discussed in the following section and in Sec.3.4.

Discussion. Silica surface ablation experiments using double-pulse irradiation have demonstrated sharp increase in LIDT for the second pulse within the delay range 67-200 fs.[12] While varying the pulse energy below the single pulse LIDT(1) the two pulse energy ratio was kept constant. The obtained results were later explained by self-trapping of the electron-hole pairs and formation of self-trapped excitons.[20] This dynamic behaviour of LIDT is faster than the 0.4 ps temporal resolution used in our experiments.

To explain our experimental data we need, first of all, to consider temporal variations of refractive index in the focal point. The low-intensity refractive index n_0, becomes modified in time due to the photoexcitation, with change $\Delta n(t)$ expressed as:

$$n_t = n_0 + \Delta n(t) = n_0 + \Delta n_{Kerr}(t) + \Delta n_{FCC}(t) + \Delta n_T(t) + \Delta n_P(t), \tag{1}$$

where $\Delta n_{Kerr} > 0$ is the Kerr nonlinearity related contribution of bound electrons, which is important on the early stages of pulse excitation while the free charge carrier (FCC) concentration is low ($< 10^{17}$ cm^{-3}). This contribution is small due to small nonlinearity of silica, $\chi^{(3)} = 3.11 \times 10^{-14}$ esu or $\chi^{(3)} = 4.34 \times 10^{-18}$ cm^2/V^2. Thus, $\Delta n_{Kerr}(t) = 2n_2\langle E^2(t)\rangle = \overline{n}_2 I(t) = \frac{3\chi^{(3)}}{4n_0^2\varepsilon_0 c} I(t) \ll n_0$ for our pulse intensities, I (in W/cm^2). Kerr contribution is at later times smeared out and overridden by the negative change of the refractive index, $\Delta n_{FCC} < 0$ due to FCC. This is the largest contribution to Δn, since absolute value of Δn_{FCC} is comparable to n_0, and will be discussed separately. The term Δn_T in eqn. 1 is the temperature related change of the refractive index, which can be expressed in terms of thermo-optical coefficient, $\partial n/\partial T$ or $\partial\epsilon/\partial T$, from Clausius-Mossotti relationship (dielectric constant $\epsilon = n^2$):[21]

$$\frac{1}{(\epsilon-1)(\epsilon+2)}\left(\frac{\partial\epsilon}{\partial T}\right) = -\alpha\left[1 - \frac{V}{\alpha_m}\left(\frac{\partial\alpha_m}{\partial V}\right)_T\right] + \frac{1}{3\alpha_m}\left(\frac{\partial\alpha_m}{\partial T}\right)_V, \tag{2}$$

where α_m is the macroscopic polarizability. The first two terms are the most important ones. The positive thermal expansion coefficient α results in negative thermo-optical coefficient. When the thermal expansion is small as in silica (indicated by high melting point, hardness, and high elastic moduli), the $\partial n/\partial T > 0$ dominated by the volume change of polarizability. In silica $\partial n/\partial T = 10^{-5}$ K$^{-1} > 0$, whereas in crystalline materials, such as quartz $\partial n/\partial T = -(2.9 \div 4)10^{-6}$ K$^{-1} < 0$ for ordinary and extraordinary beams, respectively. As can be seen, relative thermal modification of refractive index can not account for the substantial change in the index at temperatures up to the melting point, i.e. $|\Delta n_T| \ll |n_0|$ in eqn. 1. The same can be said about the last term in Eqn. 1 $\Delta n_P(t)$, which represents change of refractive index inbuced by the pressure. Moreover, the pressure wave, even if it is driven at

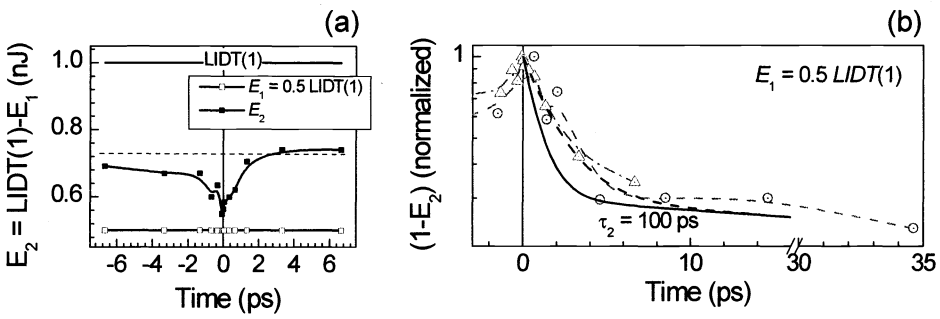

Figure 6. (a) Time dependence of the second pulse energy E_2 at 398 nm wavelength. E_2 is the energy required to reach the LIDT(2) fluence for the first pulse energy E_1 was fixed at $0.5 \times LIDT(1)$. (b) Normalized time dependence of $(1 - E_2)$, for $E_1 = 0.5 \times LIDT(1)$. Experimental data from different experiment performed under the same conditions are marked by diferent symbols. The simulated time decays (grey lines) are calculated from $y = 0.85e^{-x/\tau_1} + 0.15e^{-x/\tau_2}$, where $\tau_1 = 1$ ps, $\tau_2 = 100$ ps (grey solid line), and $\tau_1 = 2$ ps (grey dashed line).

shock velocity, which is typically twice the sound speed (4.2 km/s in silica), passes the distance equal to the lateral radius of the focal spot (359 nm) in 428 ps. This yields the temporal range within which pressure-induced refractive index changes occur.

The focusing of the second pulse is altered y the first pulse when the local index changes reach the magnitude of $\propto 0.1 \times n_0$. Assuming the main refractive index mechanism due to the free carriers, complex refractive index $\tilde{n} = n' + in''$ can be found from the Maxwell's equations given in the form:[22]

$$n' = \begin{cases} \sqrt{1 - \omega_p^2/\omega^2}, & \omega > \omega_p \\ \frac{1}{2}\frac{\nu}{\omega}\frac{\omega_p^2/\omega^2}{\sqrt{\omega_p^2/\omega^2 - 1}}, & \omega < \omega_p \end{cases} \tag{3}$$

$$n'' = \begin{cases} \frac{1}{2}\frac{\nu}{\omega}\frac{\omega_p^2/\omega^2}{\sqrt{1-\omega_p^2/\omega^2}}, & \omega > \omega_p \\ \sqrt{\omega_p^2/\omega^2 - 1}, & \omega < \omega_p \end{cases}, \tag{4}$$

where ν is the electron-phonon collision time, $\omega_p(N) = \sqrt{4\pi r_e N}c$ is the cyclic plasmon frequency dependent on the free-carrier density, and $r_e = e^2/mc^2$ is the classical electron radius expressed in terms of its charge e, mass, m, and light velocity, c. Quantities derived from Eqns. 3 and 4 are presented in Fig. 5. The refractive index variation due to free carriers become comparable to the refractive index in vicinity of plasmon resonance, where material becomes reflective (Fig. 5(c)).

The LIDT recovery within 1-10 ps can be understood as a consequence of local modification of the focusing conditions due to the refractive index change caused by free carriers. According to Fig. 4(c), free carrier relaxation can follow trace *1* or *2*. A possible explanation for the onset of the increase in the normalized $(1 - E_2)$ in Fig. 4(a) at about 10 ps is that the crossover point in the refractive index recovery is reached, according to trace *1* in Fig. 4(c). Another possibility for the explanation is in the LIDT temperature dependence, which is discussed in Sec. 3.4.

3.3. Damaging of silica by two consecutive pulses at 398 nm

LIDT recovery over similar time scale was observed in silica damaged by 398 nm pulses (Fig. 6). These results can be interpreted by the relaxation of refractive index at the focus. The free-carrier generation by the 398 nm pulse is certainly different from that discussed above, but the fast part of LIDT recovery occurs within similar time scale of 1-2 ps.

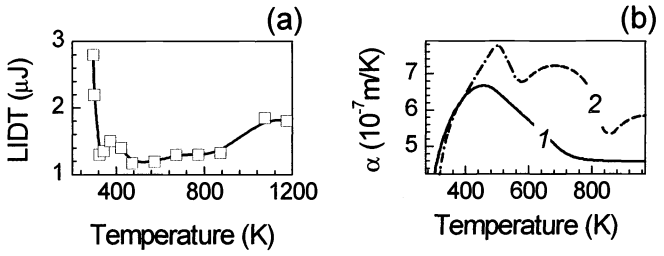

Figure 7. (a) LIDT temperature dependence. The pulse energy is measured at the entrance to the microscope. The optical damage was inflicted using 40× objective lens with $NA = 0.55$. (b) Linear thermal expansion coefficient α in fused (*1*) and synthetic (*2*) silica.

3.4. Temperature control of $LIDT(1)$

Fig. 7(a) shows the LIDT(1) dependence on the temperature. The more than two-fold decrease of LIDT can be reached by moderately elevating the temperature to $150 - 250°C$. The temperature dependence of the linear thermal expansion coefficient α in similar silica glasses is presented for comparison in Fig. 7(b). The obvious anti-correlation between $LIDT(T)$ and $\alpha(T)$ can be understood in terms of temperature-dependent molar heat capacity at constant volume C_V, and thermal conductivity, κ, (see discussion in the text).

Mechanical properties of materials are related to the optical damage. Linear thermal expansion coefficient, defined as $\alpha(T) = L^{-1}dL/dT$, where L is the length in arbitrary units, and thermal conductivity κ are temperature-dependent by definition. For isotropic glass material, the volume expansion coefficient $\alpha_V = 3\alpha$ and the Grüneisen relationship relates the thermal expansion coefficient to the molar heat capacity $\alpha(T) = \gamma C_V(T)/(3B_0V_0)$. Here B_0 and V_0 are the bulk modulus and the volume at $T = 0$ K, respectively, and $\gamma = 1 \div 2$. Thus, α has the same temperature dependence as the heat capacity at constant volume C_V. The thermal conductivity is given by $\kappa = C_V vl/3$, where v is the phonon (sound) velocity and l is the phonon mean free path. At low temperature $T \ll \theta_D$, where θ_D is Debye temperature of crystal, both α and κ increase as T^3 (Debye theory $C_V(T) \propto T^3$). At higher temperature C_V reaches the classical limit $C_V(T) \Rightarrow const$. At the same time $\kappa \propto 1/T$ at high temperature, since the phonon density is proportional to T, and consequently, $l \propto 1/T$.

The results in Fig. 7(a) show that optical damage of silica can be inflicted at lowest fluence when the linear thermal coefficient is maximized. Even for short pulses (< 1 ps) the temperature of silica target is important. As far as optical damaging using high-NA objective is concerned, fast melting and thermal quenching is important due to the small volume of the excited material, usually 1 μm^3. The spatio-temporal profile of the temperature field after the excitation by δ-shaped thermal pulse is given by the solution of the equation $\partial T/\partial t = \chi \Delta T + Const \times \delta(r)\delta(t)$, given below:[22]

$$T(r,t) = \frac{Const}{(4\pi\chi t)^{3/2}} \exp\left(-\frac{r^2}{4\chi t}\right), \tag{5}$$

where r and t are the spatial coordinate and time, respectively, and χ is the thermal conductivity. The latter can be expresed in terms of mass density ρ, heat capacity at constant pressure C_P, and thermal coductivity κ by the relation $\chi = \kappa/\rho C_P$. This suggests that the irradiation spot is expected to cool down in time according to the $T \sim t^{-3/2}$ law, and spread in space according to the $r \sim (\chi t)^{1/2}$ law. The characteristic time d^2/χ shows the time scale over which the temperature changes are expected to occur at the irradiation spot of diameter d. For silica, $\chi = 8.408 \cdot 10^{-7}$ m^2/s, and taking the diffraction-limited irradiation spot size $d = 1.22\lambda/NA = 718$ nm, one can find $d^2/\chi \simeq 610$ ns. Much faster changes were observed experimentally (Fig. 4) in the recovery of E_2. A possible explanation of these results is by nonlinear diffusion, and much smaller than expected diameter of the spot excited/heated by the first pulse.

3.5. Simulation of free carrier generation by a subpicosecond pulses

In this section we shall discuss mechanisms responsible for the electron promotion into the conduction band of silica under excitation by 440 fs pulses. Prior to that it is relevant to discuss determination of the optical breakdown threshold in some detail. From the modeling point of view, the optical breakdown of a dielectric is associated with excitation of free carriers at density equal to or above the critical density n_{cr}. In a rigorous theoretical approach the breakdown is assumed to occur above the critical laser intensity (or laser field [V/cm]) when the rate of electron energy gain from the laser field exceeds the rate of the energy loss to the lattice via the phonon scattering; or when the solid reaches the temperature close to the melting (or softening for glasses) point.[23] In our calculations we use free electron density 10^{21} cm^{-3}, which is close to the plasma frequency for 795 nm iradiation: $n_{cr} = \omega^2 m\epsilon_0/e^2 = 1.4 \times 10^{21}$ cm^{-3} , where ω is the laser angular frequency, m is the electron mass, ϵ_0 is the vacuum permitivity, and e is the electron charge. Referring to the LIDT definition given in Sect. 3.1, such silica modification exhibits signatures of very hot and dense plasma formation, accompanied by microexpolsion at the beam focus. During the pulse propagation both plasma excitation and heating must occur. Therefore, we will use $\tau_p/2$ as an estimated breakdown time (the carrier density n_{cr} is reached), regardless of whether cascade or multiphoton ionization is the dominant mechanism.

For numeric modeling of variations in the free electron density we use modified rate equation formalism derived by Stuart *et al.*.[4] Based on the transmission spectrum[19] we take the ionization potential of the ED-C brand silica to be 7.4 eV instead of commonly accepted bandgap energy of crystalline quartz silica $\Delta \simeq 9 \div 10$ eV. Photo-ionization is sensitive to the Keldysh parameter $\gamma = \omega\sqrt{m^*\Delta}/eE$, which conditionally divides the ionization process into two types: the multiphoton ionization when $\gamma \gg 1$, and the tunneling ionization when $\gamma \ll 1$; here E is the peak laser field, and m^* is the reduced electron mass evaluated as follows. The effective mass of conducting band electrons in silica can be evaluated using formulas derived from the perturbation theory $k{\cdot}p$ approach:[24]

$$\frac{m}{m^*} = 1 + \frac{2\xi^2 m d^2 V_2^2}{3\Delta\hbar^2}, \tag{6}$$

where covalent energy $V_2 = 2.16\hbar^2/(md^2)$. Here m is the electron mass, $d = 1.61$ Å is the length parameter for silica,[24] $\Delta = 7.4$ eV is the band gap energy, and scale parameter $\xi \simeq 1$. This gives $m^* \simeq 0.8m$.

Numeric calculations are most complex for $\gamma \sim 1$, when the simplifications made in the expression for the dielectric ionization probability for tunneling or multiphoton ionization are no longer valid. Under our experimental conditions Keldysh parameter varies as $\gamma = (1.1 \ldots 1.8)$. We would like to point out, that some papers dealing with dielectric breakdown do not pay attention to the importance of γ value, which is also sensitive to such material constants as the effective mass of electron and the bandgap energy. We used the following Keldysh expression for the probability of the multiphoton ionization in condensed matter[25]:

$$W = \frac{2}{9\pi}\omega\left(\frac{m^*\omega}{\hbar}\right)^{\frac{3}{2}} \exp(2K)\Phi(z)\left(\frac{1}{16}\right)^K \left[\frac{e^2 I_0}{m^*\Delta\omega^2 c\varepsilon_0 n_0}\right]^K \tag{7}$$

$$\Phi(z) = \exp(-z^2)\int_0^z \exp(y^2)dy \tag{8}$$

$$z = \sqrt{2K - \frac{2\Delta}{\hbar\omega}}, \tag{9}$$

here $K = \langle 1 + \Delta/\hbar\omega \rangle$ is the number of photons necessary to ionize silica. Using this expression the six-photon ($K = 6$) ionization rate *P(I)* can be expressed as

$$P(I) = 4.07 \times 10^{13} I_0^6 \text{ cm}^{-3}\text{ps}^{-1}, \tag{10}$$

where the peak intensity I_0 is in TW/cm^2. This value is about 3 orders of magnitude lower than that quoted in Ref. 18, but about 5 orders of magnitude exceeds that reported by Lenzner *et al.*.[2] However, it is worth to note, that smaller ionization rate assumed in our calculations does not change the qualitative picture of the interplay between the multiphoton and cascade ionization. Tunneling ionization is less important for less intense light fields.

Once free electrons are promoted into the conduction band by multiphoton absorption, they can further gain energy by single photon absorption similar to so called inverse bremsstrahlung absorption in ionized gas. The highly energetic electrons undergo momentum and energy relaxation simultaneous with absorption, during which the

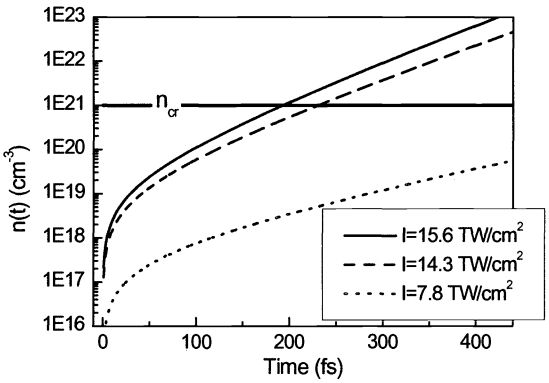

Figure 8. The dependence of the excited free electron density on the excitation time (Eqn. 12), showing the effect of the laser irradiation intensity on the temporal profile of the free electron density. The critical plasma density, n_{cr} corresponds to the optical breakdown of silica. The laser pulse duration is 440 fs (FWHM).

electron-electron and electron-phonon collisions can be assumed to be inelastic, and new electron-hole pair is created in every collision. The cascade ionization rate α per electron is given by:[26]

$$\alpha(I) = \frac{1}{\omega^2\tau^2 + 1}\left[\frac{e^2\tau}{cn\varepsilon_0 m\Delta}I_0 - \frac{m\omega^2\tau}{M}\right], \tag{11}$$

here τ is the effective electron collision time, n is the silica refractive index, and M is the mass of SiO_2 molecule. The first term is related to the electron energy gain from the electric field, while the second term describes energy transfer from electrons to heavy molecules during the elastic collisions. In our calculations we took $\tau = 2$ fs.[27] Therefore, minimum time for each doubling sequence in the avalanche is given by the product $\tau \times K = 12$ fs. If every inelastic collision is coupled with the inverse bremsstrahlung event, a cascade starting from a single seeded electron can produce $2^{440/12} = 1.4 \times 10^{11}$ free electrons in one laser pulse. This implies that the free electron density of 10^{10} cm^{-3} must be produced by multiphoton ionization to finally reach the critical electron density ρ_{cr} by avalanche. Eqns. (11) and (10) can be combined into the following expression for the conduction band electron density:[4]

$$n(t) = \left(n_{c0} + \frac{P(I)}{\alpha(I)}\right)\exp\left(\alpha(I)t\right) - \frac{P(I)}{\alpha(I)}, \tag{12}$$

where n_{c0} is the initial free electron density in the conduction band. Using this expression we can predict the electron density $n(t)$ excited during a passage of $\tau_p = 440$ fs pulse, and $\omega = 2.37 \cdot 10^{15}$ s^{-1} frequency for fixed irradiation intensity. Fig. 8 shows the temporal evolution of the free electron density following the excitation by the fs light pulse for different intensity levels: the experimentally obtained $LIDT(1)$ (solid line), the theoretical $LIDT(1)$ value considering the breakdown is reached at the half of the pulse (dashed line), and $0.5 \times LIDT(1)$ (dotted line). It follows from the theoretical calculations, that at the experimentally determined LIDT (15.6 TW/cm^2) the breakdown occurs during the first 192 fs, while the theoretical LIDT intensity is 14.3 TW/cm^2. The linear dependence of the free electron density on time in a semi-logarithmic plot in Fig. 8 proves that optical breakdown is initiated by the multiphoton ionization, which is followed and eventually completed by the cascade ionization if the pulse duration is about 0.5 ps, and the latter mechanism is more important than the multiphoton ionization. Returning to the double pulse measurements, we have checked the density of free electrons which can be excited by $0.5 \times LIDT$ intensity pulse (See Fig. 8). Our simulations yield 4.5×10^{18} cm^{-3} during the first 220 fs and about 5.6×10^{19} cm^{-3} within the entire 440 fs pulse. The resulting electron density is only two orders of magnitude smaller than the critical density. Accordingly, the intensity of the second pulse smaller than $0.5 \times LIDT$ is needed to reach the critical density ($LIDT(1)$ level). However, our experimental results in Fig. 3(a) show that the energy of the second pulse was higher than required $0.5 \times LIDT$ to reach $LIDT(1)$. This can be explained by the circumstance that the model neglects change in the refractive index experienced by the second pulse, and disregards some other processes leading to the free carrier losses, like recombination and diffusion at the focal spot. Taking into account small dimensions of the photoexcited volume, diffusion over the distances ranging from tens to hundreds of nm may be strongly pronounced.

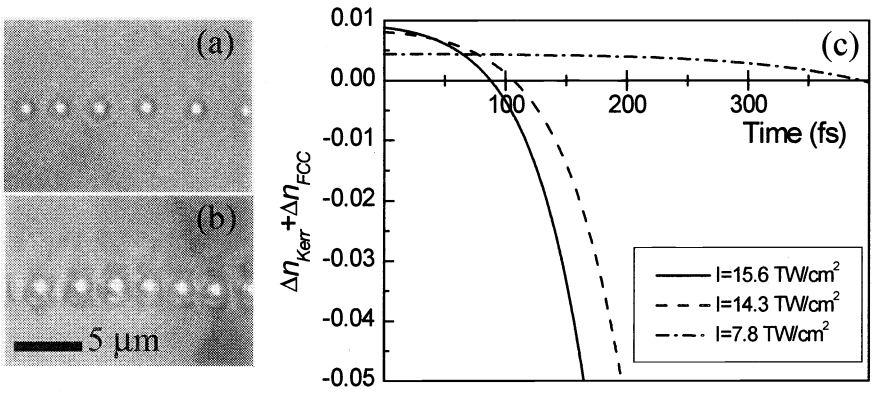

Figure 9. Transmission images of damaged spots inside silica at different fabrication pulse intensities: (a) 1.3 × LIDT (24.3 TW/cm^2) and (b) 2.2 × LIDT (34.3 TW/cm^2). (c) calculated dependence of Kerr nonlinearity and exited free carries plasma contribution to silica refractive index change during propagation of 440 fs light pulse for the same irradiation intensities as in Fig.8.

Absorption by free holes is another important factor not considered in this model, basically due to the lack of data. Valence band holes can be heated to the energies sufficient for the impact ionization. Our simulations give correct qualitative picture of the optical breakdown, and the experimentally observed values of LIDT are corroborated numerically.

Results of numeric simulation of free carrier excitation dynamics allow us to reveal the variations of the refractive index in silica during fs pulse propagation. The complex refractive index variation in plasma is quantitatively described by means of the laser-induced plasma index modulation[28]

$$\Delta n_{FCC}(t) = \frac{2e^2\tau}{n_0 m\omega}\left(\frac{(1-\omega^3\tau^3)+i(\omega^2\tau^2+\omega\tau)}{\omega^4\tau^4+1}\right)\times n(t) \tag{13}$$

Thus, the plasma formation causes decrease in the real part of the medium refractive index explained by Eq.13, and acts as a concave lens, while influence of Kerr nonlinearity has an opposite effect and causes beam self-focusing. The interplay between these effects could be accounted for in numerical modeling by the combination of Eq. 12 and Eq. 13. The results of numerical simulation for the same intensity levels as in LIDT calculation were shown in Fig.9(c). According to our simulation, silica refractive index was decreased during the propagation of fs pulse of 0.5×LIDT(1) intensity. This indicates, that focusing conditions for the second pulse should be different even if the electron density in the conduction band is not sufficient for the permanent silica damage. Furthermore, at intensities ≥ LIDT(1), plasma defocusing is more pronounced (Fig.9(c)), and this is one of the possible explanations why we have observed increase in the diameter of the damaged spot Fig.9(a-b) at higher irradiation intensities.

4. CONCLUSIONS

The presented investigation of LIDT by sub-picosecond pulses in bulk silica demonstrates that 350 fs laser pulses focused by a high-NA microscope objective yield one of the lowest reported values of LIDT for a single shot regime, 5 J/cm^2 , which is well below the critical self-focusing power. We find that the decay of the free carrier plasma excited by 440 fs pulses is approximately exponential with time constant of 2 ps, much longer than that reported by Li *et al.*.[12] For silica lattice temperature up to 400 K (the point of maximum linear thermal expansion coefficient), the single-shot LIDT decreases with temperature. Finally, photoluminescence spectra of silica optically damaged by ps-pulses are found to be similar to those of silica, damaged by femtosecond pulses, and subsequently annealed at 1050-1100°C temperature.

These findings demonstrate that in experiments with two mutually delayed pulses of sub-threshold intensity decrease of LIDT for the second pulse can be expected, provided that substantial local heating or density of free carriers created by the first pulse persist until the arrival of the second pulse to the damage spot.

ACKNOWLEDGMENTS

This work was in part supported by the Satellite Venture Business Laboratory of the University of Tokushima.

REFERENCES

1. D. Du, X. Liu, G. Korn, J. Squier, and G. Mourou, "Laser-induced breakdown by impact ionization in SiO_2 with pulse widths from 7 ns to 150 fs," *Appl. Phys. Lett.* **64**, pp. 3071–3073, 1994.
2. M. Lenzner, J. Kruger, S. Sartania, Z. Cheng, C. Spielmann, G. Mourou, W. Kautek, and F. Krausz, "Femtosecond optical breakdown in dielectrics," *Phys. Rev. Lett.* **80**, pp. 4076–4079, 1998.
3. A. C. Tien, S. Backus, H. Kapteyn, M. Murnane, and G. Mourou, "Short-pulse laser damage in transparent materials as a function of pulse duration," *Phys. Rev. Lett.* **82**, pp. 3883–3886, 1999.
4. B. C. Stuart, M. D. Feit, S. Herman, A. M. Rubenchik, B. W. Shore, and M. D. Perry, "Nanosecond to femtosecond laser induced breakdown in dielectrics," *Phys. Rev. B* **53**, pp. 1749–1441, 1996.
5. B. C. Stuart, M. D. Feit, A. M. Rubenchik, B. W. Shore, and M. D. Perry, "Laser-induced damage in dielectrics with nanosecond to subpicosecond pulses," *Phys. Rev. Lett.* **74**, pp. 2248–2251, 1995.
6. T. Apostolova and Y. Hahn, "Modelling of laser-induced breakdown in dielectrics with subpicosecond pulses," *J. Appl. Phys.* **88**, pp. 1024–1034, 2000.
7. A. Vaidyanathan, T. W. Walker, and A. H. Guenther, "The relative roles of avalanche multiplication and multiphoton absorbtion in laser-induced damage in dielectrics," *IEEE J. Quantum Electron.* **16**, pp. 89–93, 1980.
8. N. Bloembergen, "Laser-induced electric breakdown in solids," *IEEE J. Quantum Electron.* **10**, pp. 375–386, 1974.
9. E. N. Glezer and E. Mazur, "Ultrafast-laser driven micro-explosions in transparent materials," *Appl. Phys. Lett.* **71**, pp. 882–884, 1997.
10. M. Watanabe, H. Sun, S. Juodkazis, T. Takahashi, S. Matsuo, Y. Suzuki, J. Nishii, and H. Misawa, "Three-dimensional optical data storage in vitreous silica," *Jpn. J. Appl. Phys.* **37**, pp. L1527–L1530, 1998.
11. H. Misawa, H. B. Sun, S. Juodkazis, M. Watanabe, and S. Matsuo, "Microfabrication by femtosecond laser irradiation," *Proc. SPIE* **3933**, pp. 246–260, 2000.
12. M. Li, S. Menon, J. P. Nibarger, and G. N. Gibson, "Ultrafast electron dynamics in femtosecond optical breakdown in dielectrics," *Phys. Rev. Lett.* **82**, pp. 2394–2397, 1999.
13. P. Martin, S. Guizard, P. Daguzan, and G. Petite, "Subpicosecond study of carrier trapping dynamics in wide-band-gap crystals," *Phys. Rev. B* **55**(9), pp. 5799–5810, 1997.
14. K. Shimakawa, A. Kolobov, and S. R. Elliott, "Photoinduced effects and metastability in amorphous semiconductors and insulators," *Adv. Phys.* **44**(6), pp. 475–588, 1995.
15. N. Matsunami and H. Hosono, "Bi-self-trapped-exciton model for frenkel defect formation in amorphous SiO_2 by proton irradiation," *Phys. Rev. B* **60**(15), pp. 10616–10619, 1999.
16. C. B. Schaffer, N. Nishimura, and E. Mazur, "Thresholds for femtosecond laser-induced breakdown in bulk transparent solids and water," in *Time structure of X-ray sources and its applications*, A. K. Freund, H. P. Freund, and R. M. Howells, eds., *Proc. SPIE* **3451**, pp. 2–8, 1998.
17. D. Ashkenasi, M. Lorenz, R. Stoian, and A. Rosenfeld, "Surface damage threshold and structuring of dielectrics using femtosecond laser pulses: the role of incubation," *Appl. Surf. Sci.* **150**, pp. 101–106, 1999.
18. C. Quoix, G. Grillon, A. Antonetti, J.-P. Geindre, P. Auderbert, and J. C. Gauthier, "Time-resolved studies of short pulse laser-produced plasmas in silicon dioxide near breakdown threshold," *Eur. Phys. J. AP* **5**, pp. 163–169, 1999.
19. S. Juodkazis, A. Marcinkevičius, M. Watanabe, V. Mizeikis, S. Matsuo, and H. Misawa, "Sub-picosecond optical damaging of silica: time resolved measurements of light induced damage threshold," in *Proc. of XXXII Ann. Symp. on Optical Materials for High Power Lasers. Boulder, U.S.A., Oct.16-18, 2000.*, 2000 (In press).
20. G. Petite, S. Guizard, P. Martin, and F. Quere, "Comment on "Ultrafast electron dynamics in femtosecond optical breakdown of dielectrics"," *Phys. Rev. Lett.* **83**, p. 5182, 1999.
21. M. Bass, ed., *Handbook of optics. Devices, Measurements, and Properties*, vol. II, McGraw-Hill, New York, 1995.
22. N. I. Koroteev and I. L. Shumai, "Physics of intense laser radiation," *Nauka, Moscow* , 1991 (In Russ.).
23. D. Arnold and E. Cartier, "Theory of laser-induced free-electron heating and impact ionization in wide-band-gap solids," *Phys. Rev. B* **46**, pp. 15102–15115, 1992.
24. W. A. Harrison, *Electronic structure and the properties of solids. The physics of the chemical bond.*, ch. 11, Mixed tetrahedral solids, pp. 257–288. Dover Publications, Inc., 1989.
25. L. V. Keldysh, "Ionization in the field of a strong electromagnetic wave," *Sov. Phys. JETP* **20**, pp. 1307–1314, 1965.
26. P. K. Kennedy, "A first-order model for computation of laser-induced breakdown thresholds in ocular and aqueous media: part I- theory," *IEEE J. Quantum Electron.* **31**, pp. 2241–2249, 1995.
27. P. P. Pronko, P. A. VanRompay, C. Horvath, F. Loesel, T. Juhasz, X. Liu, and G. Mourou, "Avalanche ionization and dielectric breakdown in silicon with ultrafast laser pulses," *Phys. Rev. B* **58**, pp. 2387–2390, 1998.
28. S. H. Cho, H. Kumagai, K. Midorikawa, and M. Obara, "Fabrication of double cladding structure in optical multimode fibers using plasma channeling excited by high-intensity femtosecond laser," *Opt. Commun.* **168**, pp. 287–295, 1999.